12-2017

Extended LaMer Synthesis of Cobalt Doped Ferrite

Benjamin D. Fellows
Clemson University

Sarah Sandler
Clemson University

Jacob Livingston
Clemson University

Kristin Fuller
Clemson University

Lotanna Nwandu
Rose-Hulman Institute of Technology

See next page for additional authors

Authors
Benjamin D. Fellows, Sarah Sandler, Jacob Livingston, Kristin Fuller, Lotanna Nwandu, Sarah Timmis, Kayla A. Lantz, Morgan Stefik, and O. Thompson Mefford

Article Subject Biomagnetics

Extended LaMer Synthesis of Cobalt Doped Ferrite

Benjamin D. Fellows[1], Sarah Sandler[1], Jacob Livingston[2], Kristin Fuller[1], Lotanna Nwandu[4], Sarah Timmins[1], Kayla A. Lantz[3], Morgan Stefik[3], O. Thompson Mefford[1]

[1] *Department of Materials Science and Engineering, Center for Optical Materials Science and Engineering Technology (COMSET), Clemson University, Anderson, SC 29625, USA*

[2] *Department of Bioengineering, Clemson University, Clemson, SC 29634, USA*

[3] *Department of Chemistry and Biochemistry, University of South Carolina, Columbia, SC 29208, USA*

[4] *Department of Biology and Biomedical Engineering, Rose-Hulman Institute of Technology, Terre Haute, IN, USA*

Received 1 Apr 2016, revised 15 Apr 2016, accepted 20 Apr 2016, published 1 Jun 2016, current version 15 Jun 2016. (Dates will be inserted by IEEE; "published" is the date the accepted preprint is posted on IEEE Xplore®; "current version" is the date the typeset version is posted on Xplore®).

Abstract— Non-stoichiometric cobalt ferrite nanoparticles have drawn interest in magnetically mediated energy delivery due to their high magnetocrystalline anisotropy and their high peak loss frequency. The use of an extended LaMer synthesis allows for size control of the doped particles up to a threshold core diameter of 18nm. Above this diameter particles become unstable and drop out of suspension allowing for further nucleation events to occur. This leads to an cyclic nucleation, growth, and destabilization regimes seen during the course of the reaction. Using the size control of the extended LaMer synthesis technique we examine the specific absorption rate (SAR) as a function of particle size up to 18 nm and observe the same oscillatory behavior in the measured SAR values.

Index Terms—Cobalt ferrite, MagMED, Hyperthermia, Magnetic nanoparticle, Specific absorption rate.

I. INTRODUCTION

Magnetically mediated energy delivery (MagMED), also referred to as magnetic field hyperthermia, has been a heavily researched area in the magnetic community for many years[1-5]. With this technique, an alternating magnetic field is applied to magnetic particles. The particles then convert the energy of the magnetic field and deliver it locally to the surrounding medium. One method to measure the efficiency of this transfer is defined by the specific absorption rate (SAR) of the material which can be quantified by placing a sample in an alternating field and measuring the temperature change of the medium over time. The energy produced during this time period is related to both the frequency (number of cycles) and the field magnitude as each field flip can be seen as a minor hysteresis loop with the area of the loop being the energy released in a single magnetization event[6]. To maximize the area in these minor hysteresis loops, two main properties can be manipulated. The first is the effective anisotropy, which is an intrinsic value based on the material composition, and the second is particle volume. The chosen field and frequency, as well as the investigated material, influence the optimal volume [6]. The ability to control and change effective anisotropy and particle volume present a unique opportunity to produce materials that can be optimized for maximum power output at a given field and frequency.

Traditionally, research in MagMED has been centered on the most commonly studied iron oxide phases, maghemite (γ-Fe_2O_3) and magnetite (Fe_3O_4). Despite significant research activity, there are currently limited commercial and clinical applications of these materials. Recently, to improve upon the material properties of iron oxides, researchers have begun to consider substituted and doped ferrites[7-11]. These materials show a wide range of magnetic properties, including, tunable magnetic saturation, magnetocrystalline anisotropy, and blocking temperature[12]. Coupled with recent advancements in synthesis, and increasing control over both size and morphology of nanoscale colloids, these new materials have been shown to exhibit properties that are greatly improved from those of Fe-ferrites. One of these select materials is cobalt ferrite ($CoFe_2O_4$), which has a much greater effective anisotropy due to the replacement of the Fe^{2+} with the highly anisotropic Co^{2+} ions[13, 14]. By maximizing the effective anisotropy through Co doping, specifically between cobalt levels between 0.4 and 1 in $Co_xFe_{3-x}O_4$, as well as identifying the optimal volume for energy release using a novel extended LaMer synthesis, the optimization of cobalt ferrite based materials for application in MagMED is possible[15, 16]. Herein, we describe a potential synthetic method to produce these materials in a size controllable manor, and the resulting properties of the particles relating to MagMED.

II. Materials and Methods

A. Extended LaMer Drip Synthesis

Metal oleates were synthesized by combining 9.3 mmol of metal acetylacetonate and 15 ml of oleic acid. The reaction was initially purged and performed under constant (<50 ml/min) nitrogen flow. The reaction was heated to 320 °C for 20 minutes and then removed from the heating source, yielding a viscous, oily liquid with no magnetic response. Fourier-transform infrared spectroscopy was performed to confirm the presence of the oleate complex and the minimization of the free acid peak at 1710 cm^{-1} and the appearance of the carboxylate anion with peaks at 1578 cm^{-1} and 1440 cm^{-1}[15].

The metal oleate precursors were diluted to 0.22 M in octadecene to help with injection. Diluted precursors were combined in predetermined 1:5 cobalt to iron molar ratios. $Co_{0.5}Fe_{2.5}O_4$ was chosen because initial reactions suggested optimal properties for the maximization of SAR for the setup used. The precursor mixture was loaded into a 10 ml syringe attached to a penetration needle, and affixed to a syringe pump. The 3-neck flask was loaded with 2.5 g of docosane and 2.5 ml of oleic acid and heated to 350 °C under inert (nitrogen) atmosphere. When the solution temperature was stable, the

Corresponding author: O. Thompson Mefford (mefford@clemson.edu). Digital Object Identifier: 10.1109/LMAG.XXXX.XXXXXXX (inserted by IEEE).

precursor solution was added at a rate of 3 ml/hr. Aliquots were taken between 20 and 120 minutes in 5 minute increments by pipetting ~100 µl of the solution out of the flask and into a 1 ml scintillation vial.

B. Attenuated Total Reflectance-Fourier Transform Infrared Spectroscopy

Attenuated total reflectance Fourier transform infrared (ATR-FTIR) spectroscopy was done using a Thermo-Nicolet Magna 550 FTIR spectrometer. 16 Scans were done for both the sample and the background. Samples were prepped by dropping a small amount of the oleate sample onto a diamond crystal. Crystal contact was assumed to be good due to the liquid nature of the sample.

C. Transmission Electron Microscopy

Bright field transmission electron microscopy was run on a Hitachi H7600 with a variable spot size operating at 120 keV. Image analysis was done using Image J (NIH, open-source) on a minimum of 300 particles.

D. AC Calorimetry

Specific absorption rate (SAR) measurements on particles were done using a field of 38 kAm^{-1} at a frequency of 206 kHz. A sample containing 500 µl of purified particles in toluene were transferred into a 1ml glass vial. The vial was inserted into the water jacket contained within the coil and an optical temperature probe was submerged into the toluene solution. Toluene was used to minimize evaporation between runs. The water jacket temperature was set to 37 °C. Once the sample temperature was stable, the power source was turned on and run for 120 s. The rise in temperature was recorded as a function of time and the average initial slope based on the first 40 seconds of three separate heating runs was used in calculating the specific absorption rate.

E. Inductively Coupled Plasma Optical Emission Spectroscopy (ICP-OES)

ICP-OES was run using a Perkin Elmer Optima 3100 ICP-OES running WinLab32 version 3.1 analysis software. Particle samples were digested initially with 30% hydrogen peroxide solution (Sigma-Aldrich) to remove organic. The peroxides were boiled off and the remaining inorganic was digested with <70% nitric acid (ARISTAR PLUS, VWR). The nitric acid was boiled off and the resulting nitrate salts were dissolved in a known mass of 2% nitric acid solution and run against standard solutions.

F. Small-angle X-ray Scattering

Small-angle X-ray scattering (SAXS) experiments were conducted using a SAXS LAB Ganesha at the South Carolina SAXS Collaborative at the University of South Carolina. A Xenocs GeniX3D microfocus source was used with a copper target to generate a monochromatic beam with a 0.154 nm wavelength. The instrument was calibrated using silicon powder (NIST 640e). Scattering data were processed from the scattering vector $q=4\pi\lambda^{-1}\sin\theta$ where λ is the X-ray wavelength and 2θ is the total scattering angle. A 300K Pilatus detector (Dectris) was used to collect the two-dimensional (2D) scattering patterns. SAXS GUI software was used for radial integration of the acquired 2D patterns to reduce the data to 1D profiles. Sample solutions were prepared by diluting the crude reaction product to <5 vol% in hexane to avoid structure factor contributions to the scattering curve.

Samples were passed through a 200 µm syringe filter just prior to measurement in a sealed glass capillary. A blank sample consisting of a capillary with only hexanes was measured under the same conditions for background subtraction using SAXS GUI. All samples were acquired for 15 minutes at room temperature with an incident X-ray flux of ~21.4 M photons per second.

G. Small Angle X-ray Fitting

Nanoparticle dimension distributions were determined by fitting each SAXS data as a Gaussian number distribution of hard spheres. Custom MATLAB R2014a programs were used for the analysis. Here, the scattering intensity, I(q), for a single sphere of radius R is

$$I(q) = \rho_0^2 v^2 \frac{9(sinqR - qRcosqR)^2}{(qR)^6} \quad (1)$$

where ρ_0 is the electron density contrast, and v is the volume of the sphere, respectively. The total scattering curve was calculated as a sum across a Gaussian distribution, taking into account both the scattering strength and the relative abundance of each sphere radius sampled. The fitting was performed by minimizing the residuals on a $\log(Iq^4)$ vs q basis. The data was well fit by modeling form factors alone.

III. Results and Discussion

A. Extended LaMer Synthesis

Metal oleate complexes used for the extended LaMer synthesis were produced via a truncated one-pot synthesis as is described by Vreeland et al. Initial data suggested that particle nucleation and formation began approximately 40 minutes into the reaction equating to 2 ml of 0.22 M precursor (44 µmols) with the first measurable SAR value occurring at 50 minutes when particle size was 10.8 nm (657 nm^3). Growth of particles continued up to 80 minutes, reaching a final diameter of 21.5 nm (5225 nm^3) with a sharp decrease in particle diameter to 14.8 nm (volume 1683 nm^3) at 85 minutes. This drop may correlate with the sudden decrease in the SAR value at the 85 minute time point as seen in figure 1.

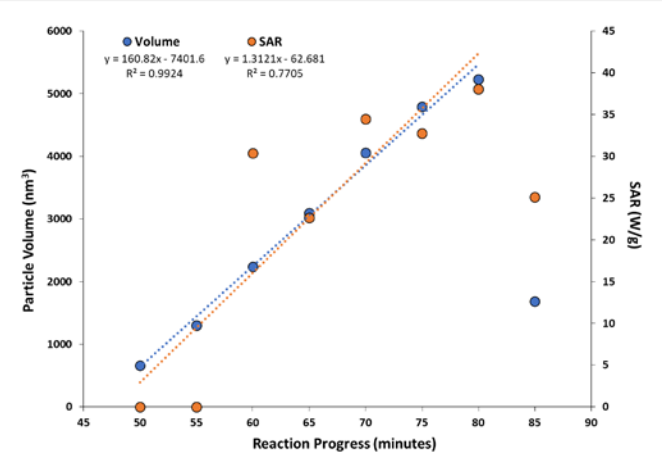

Figure 1. Extended LaMer growth of $Co_{0.5}Fe_{2.5}O_4$ nanoparticles over time with particle volume determined by SAXS analysis compared to SAR values. Particle volume is linear up to 85 minutes. SAR shows no discernable trend. Linear best fit lines exclude the last point in the data shown.

SAXS analysis of this extended LaMer growth ($Co_{0.5}Fe_{2.5}O_4$) was consistent with linear volumetric growth with time of 160.8 nm^3/min with an R^2 value of 0.99 and a sudden decrease in nominal particle size at 85 minutes. The best-fit line indicated an induction time of 46 minutes prior to the start of growth, although this may not

account for possible initial rapid catalytic growth via the Finke-Watzky mechanism.[15]

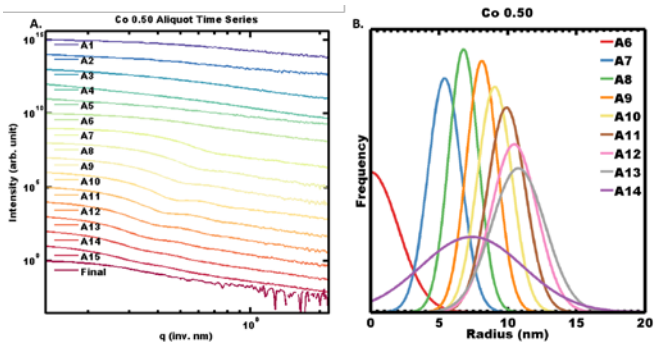

Figure 2. SAXS data for the extended LaMer drip of $Co_{0.5}Fe_{2.5}O_4$. A1 corresponds to 20 minutes into the reaction. Aliquots were taken every 5 minutes up until the final at 95 minutes. A) Intensity vs scattering vector (q) as the reaction progresses. B) Size distribution of particles at particular aliquots showing particle growth. Scattering data was first able to be fit at A6 showing small crystallites using a truncated gaussian. Subsequent aliquots show small dispersion until A14 where the distribution widens and shifts to a lower diameter.

The observed decrease in average particle size may occur as a result of reaching a critical size at which the nanoparticles precipitate from solution and the further subsequent addition of precursors results in secondary nucleation. This is of high importance as it shows that the extended LaMer synthesis for magnetite ported to a more complex ferrite system and needs to be fine-tuned to support each material on a case-by-case basis. Although this instability was observed, SAXS and TEM data shows that $Co_{0.5}Fe_{2.5}O_4$ particles with diameters between 10nm and 18 nm can be synthesized reliably using this method without major colloidal instabilities. SAXS data for the LaMer reaction shown in figure 2.

The instability of the particles at approximately 18 nm also leads to an interesting phenomenon where a secondary nucleation phase occurs. This is illustrated in figure 3D where we see the TEM images and the corresponding size analysis show a bimodal distribution with the primary distribution falling around the smaller (6 nm) diameter particles and a secondary distribution at a much larger size (17 nm). This may be in part due to the destabilization of particles happening at a fast enough rate that growth kinetics of particles still in solution cannot consume free metal monomer fast enough, allowing for a buildup in monomer concentration. This may lead to secondary nucleation event. Initial attempts at remedying this issue were made by lowering flow rate of the precursor injection. A 1 ml/hr flow rate caused issues with the synthesis itself as both the slow flow of N_2 gas and taking usable aliquots caused the reaction to "dry up" before meaningful data could be extracted. The 2 ml/hr flow rate produced particles that were inhomogeneous in both shape and size further exacerbating the issue with the inhomogeneity seen in the 3 ml/hr drip rate. It must be noted

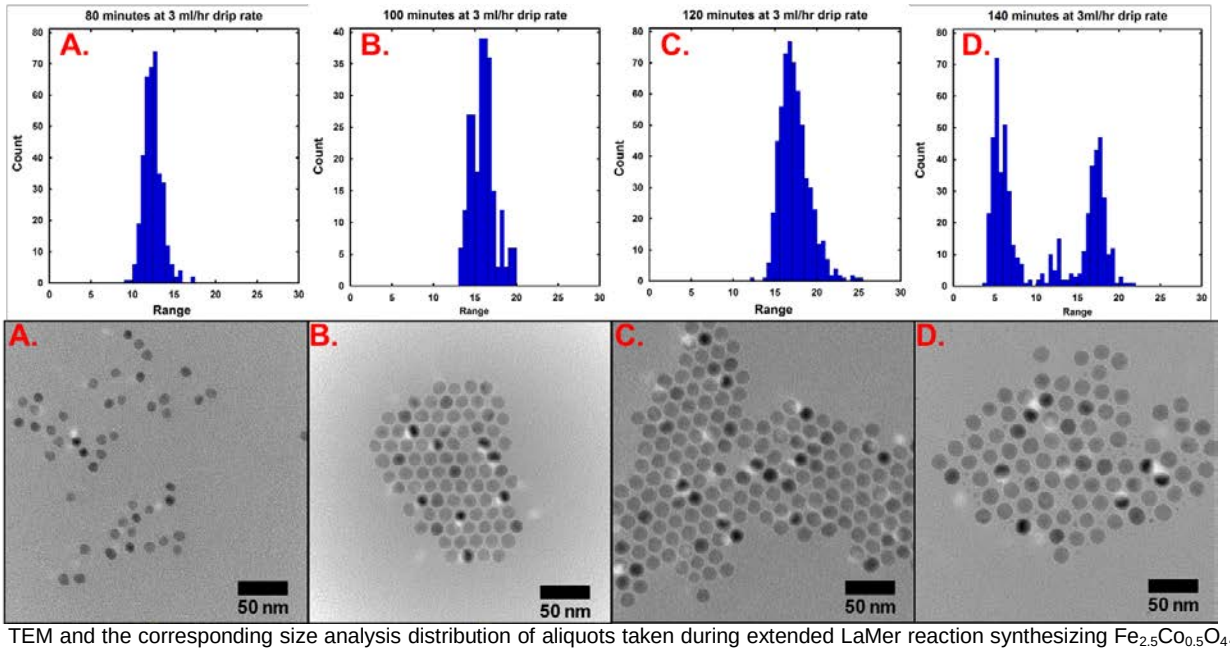

Figure 3. TEM and the corresponding size analysis distribution of aliquots taken during extended LaMer reaction synthesizing $Fe_{2.5}Co_{0.5}O_4$. A) 80 minutes diameter=12.4 nm, standard deviation=1.1 nm. B) 100 minutes, diameter= 16.0 nm, standard deviation= 1.4 nm. C) 120 minutes diameter= 17.4 nm, standard deviation= 1.8 nm. D) 140 minutes, diameter small= 6.54 nm, standard deviation small= 2.3 nm, diameter large= 17.4 nm, standard deviation large= 1.2 nm. All scale bars are 50 nm.

that there are many additional variables to change including precursor concentration, capping ligand concentration, reaction temperature etc. and that exploration into the optimization of this synthesis is ongoing.

B. SAR vs. Particle Size

One of the many advantages in using an extended LaMer synthesis is that particle size can be controlled, and once a desired size is reached, the reaction can be quenched yielding a sample with relatively low dispersion and high uniformity. Alternatively, small aliquots can be taken throughout the reaction to isolate size as a lone variable. Expectedly as the reaction proceeds, the particles get larger and the SAR of the samples increases which can be seen in Figure 1. However, the SAR values calculated from the drip reaction aliquots were surprisingly low, with the highest at approximately 50 W/g.

It is important to note that the diameters given in this manuscript (both TEM and SAXS) may not represent the true magnetic diameter. The particles may contain a relatively large magnetic dead layer which has been seen in iron oxide particles, which may explain the

low SAR values exhibited by these particles[17]. The low SAR values may also be artificially lowered due to the presence of unreacted precursor still left in the sample during measurement. Because of the constant drip of oleate precursor it is inevitable that some is taken up in each of the aliquots. Although chromatography was done to try and minimize this, it is difficult to fully separate all excess oleic acid and metal oleate from the particle sample. Any excess metal not incorporated into a particle would not contribute to the heating rate during calorimetry but would show up in the mass normalization, thus leading to an artificially low specific absorption rate. A longer drip reaction was run to confirm the SAR value limit as well as to see the effects of the secondary nucleation. As the reaction progressed an expected increase and unexpected sudden drop in SAR was seen, similar to previous reactions. What is interesting to note is that a secondary increase and sudden drop in SAR was seen again after the first SAR increase and decrease cycle. This illustrates that the drip reaction under these conditions ($Fe_{2.5}Co_{0.5}O_4$ @ 3ml/min) showed an almost oscillatory effect through nucleation growth and destabilization seen in figure 4. These phenomena limit the usefulness in using this specific reaction with these parameters to synthesize large diameter particles but applications looking for size control of cobalt doped ferrites within the 10 to 20 nm regime may find the presented synthesis useful.

Investigation into different ligands, drip rates and precursor concentrations could potentially alleviate the secondary nucleation by changing the energetics allowing the particles to stay in solution, or change the metal monomer addition rates to eliminate secondary monomer buildup and nucleation.

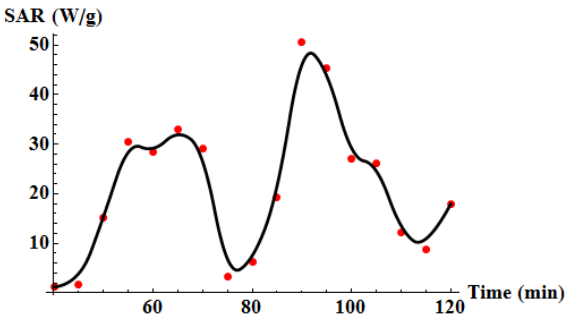

Figure 4. Extended specific absorption rate as a function of reaction time showing oscillatory behavior from multiple nucleation, growth, and precipitation cycles.

IV. CONCLUSION

This study has demonstrated the viability of uniformly incorporating defined percentages of cobalt into ferrite based nanoparticles and illustrates the use of the extended LaMer synthesis in the ability to control size of cobalt ferrite nanoparticles. Further exploration into the experimental drip procedure must be done to optimize the synthesis as particle stability above 22 nm, and unwanted nucleation events were shown. Initial experiments into changing the flow rate of precursor show promise but a more detailed exploration of drip rate, precursor concentration, and stabilizing ligand are necessary.

V. ACKNOWLEDGMENT

A special thank you to Jessica Bigner from Clemson University for her help with initial experiments and imaging leading up to the extended LaMer synthesis work. We would also like to thank Dr. Martin Saunders, from the University of Western Australia, for his imaging expertise. The authors would like to acknowledge the support of the Clemson Creative Inquiry Program and Calhoun Honors College. This work made use of the South Carolina SAXS Collaborative, supported by the NSF Major Research Instrumentation program (award #DMR-1428620). We thank Dr. Gila Stein at the University of Tennessee, Knoxville for the helpful SAXS fitting discussions. The authors would also like to acknowledge the facilities, and the scientific and technical assistance of the Australian Microscopy & Microanalysis Research Facility at the Centre for Microscopy, Characterization & Analysis, The University of Western Australia, a facility funded by the University, State and Commonwealth Governments.

VI. REFERENCES

[1] J. R. Oleson, "A Review of Magnetic Induction Methods for Hyperthermia Treatment of Cancer," *Ieee Transactions on Biomedical Engineering,* vol. 31, pp. 91-97, 1984.

[2] Q. A. Pankhurst, J. Connolly, S. K. Jones, and J. Dobson, "Applications of magnetic nanoparticles in biomedicine," *Journal of Physics D-Applied Physics,* vol. 36, pp. R167-R181, Jul 7 2003.

[3] Q. A. Pankhurst, N. T. K. Thanh, S. K. Jones, and J. Dobson, "Progress in applications of magnetic nanoparticles in biomedicine," *Journal of Physics D-Applied Physics,* vol. 42, Nov 21 2009.

[4] C. C. Berry and A. S. G. Curtis, "Functionalisation of magnetic nanoparticles for applications in biomedicine," *Journal of Physics D-Applied Physics,* vol. 36, pp. R198-R206, Jul 7 2003.

[5] C. C. Berry, "Progress in functionalization of magnetic nanoparticles for applications in biomedicine," *Journal of Physics D-Applied Physics,* vol. 42, Nov 21 2009.

[6] J. Carrey, B. Mehdaoui, and M. Respaud, "Simple models for dynamic hysteresis loop calculations of magnetic single-domain nanoparticles: Application to magnetic hyperthermia optimization," *Journal of Applied Physics,* vol. 109, p. 083921, 2011.

[7] V. M. Khot, A. B. Salunkhe, N. D. Thorat, R. S. Ningthoujam, and S. H. Pawar, "Induction heating studies of dextran coated MgFe2O4 nanoparticles for magnetic hyperthermia," *Dalton Trans,* vol. 42, pp. 1249-58, Jan 28 2013.

[8] A. Iftikhar, M. U. Islam, M. S. Awan, M. Ahmad, S. Naseem, and M. Asif Iqbal, "Synthesis of super paramagnetic particles of Mn1−xMgxFe2O4 ferrites for hyperthermia applications," *Journal of Alloys and Compounds,* vol. 601, pp. 116-119, 2014.

[9] T. Kondo, K. Mori, M. Hachisu, T. Yamazaki, D. Okamoto, M. Watanabe*, et al.*, "Alternating current magnetic susceptibility and heat dissipation by Mn1−xZnxFe2O4 nanoparticles for hyperthermia treatment," *Journal of Applied Physics,* vol. 117, p. 17D157, 2015.

[10] S. Sabale, V. Jadhav, V. Khot, X. Zhu, M. Xin, and H. Chen, "Superparamagnetic MFe2O 4 (M = Ni, Co, Zn, Mn) nanoparticles: synthesis, characterization, induction heating and cell

viability studies for cancer hyperthermia applications," *J Mater Sci Mater Med,* vol. 26, p. 127, Mar 2015.

[11] G. Stefanou, D. Sakellari, K. Simeonidis, T. Kalabaliki, M. Angelakeris, C. Dendrinou-Samara*, et al.*, "Tunable AC Magnetic Hyperthermia Efficiency of Ni Ferrite Nanoparticles," *Ieee Transactions on Magnetics,* vol. 50, Dec 2014.

[12] B. Fischer, J. Wagner, M. Schmitt, and R. Hempelmann, "Tuning the relaxation behaviour by changing the content of cobalt in CoxFe3−xO4 ferrofluids," *Journal of Physics: Condensed Matter,* vol. 17, pp. 7875-7883, 2005.

[13] A. López-Ortega, E. Lottini, C. d. J. Fernández, and C. Sangregorio, "Exploring the Magnetic Properties of Cobalt-Ferrite Nanoparticles for the Development of a Rare-Earth-Free Permanent Magnet," *Chemistry of Materials,* vol. 27, pp. 4048-4056, 2015.

[14] E. Fantechi, G. Campo, D. Carta, A. Corrias, C. de Julián Fernández, D. Gatteschi*, et al.*, "Exploring the Effect of Co Doping in Fine Maghemite Nanoparticles," *The Journal of Physical Chemistry C,* vol. 116, pp. 8261-8270, 2012.

[15] E. C. Vreeland, J. Watt, G. B. Schober, B. G. Hance, M. J. Austin, A. D. Price*, et al.*, "Enhanced Nanoparticle Size Control by Extending LaMer's Mechanism," *Chemistry of Materials,* vol. 27, pp. 6059-6066, 2015.

[16] A. Franco and V. Zapf, "Temperature dependence of magnetic anisotropy in nanoparticles of CoxFe(3−x)O4," *Journal of Magnetism and Magnetic Materials,* vol. 320, pp. 709-713, 2008.

[17] M. Unni, A. M. Uhl, S. Savliwala, B. H. Savitzky, R. Dhavalikar, N. Garraud*, et al.*, "Thermal Decomposition Synthesis of Iron Oxide Nanoparticles with Diminished Magnetic Dead Layer by Controlled Addition of Oxygen," *ACS Nano,* vol. 11, pp. 2284-2303, Feb 28 2017.